



HAL
open science

Microgrid sizing with combined evolutionary algorithm and MILP unit commitment

Bei Li, Robin Roche, Abdellatif Miraoui

► **To cite this version:**

Bei Li, Robin Roche, Abdellatif Miraoui. Microgrid sizing with combined evolutionary algorithm and MILP unit commitment. *Applied Energy*, 2017, 188, pp.547 - 562. hal-02131005

HAL Id: hal-02131005

<https://hal.science/hal-02131005>

Submitted on 16 May 2019

HAL is a multi-disciplinary open access archive for the deposit and dissemination of scientific research documents, whether they are published or not. The documents may come from teaching and research institutions in France or abroad, or from public or private research centers.

L'archive ouverte pluridisciplinaire **HAL**, est destinée au dépôt et à la diffusion de documents scientifiques de niveau recherche, publiés ou non, émanant des établissements d'enseignement et de recherche français ou étrangers, des laboratoires publics ou privés.

Microgrid sizing with combined evolutionary algorithm and MILP unit commitment

Bei Li^{a,*}, Robin Roche^a, Abdellatif Miraoui^b

^aFEMTO-ST, UMR CNRS 6174, and FCLAB, FR CNRS 3539, Université Bourgogne Franche-Comté, Belfort / UTBM, 90000, France

^bUniversité Bourgogne Franche-Comté / UTBM, Belfort / UTBM, 90000, France

Abstract

Microgrids are small scale power systems with local resources for generation, consumption and storage, that can operate connected to the main grid or islanded. In such systems, optimal sizing of components is necessary to ensure secure and reliable energy supply to loads at the least cost. Sizing results are however dependent on the energy management strategy used for operating the system, especially when components with different dynamics are considered. Results are also impacted by uncertainty on load as well as renewable generation. In this paper, we propose a combined sizing and energy management methodology, formulated as a leader-follower problem. The leader problem focuses on sizing and aims at selecting the optimal size for the microgrid components. It is solved using a genetic algorithm. The follower problem, i.e., the energy management issue, is formulated as a unit commitment problem and is solved with a mixed integer linear program. Uncertainties are considered using a form of robust optimization method. Several scenarios are modeled and compared in simulations to show the effectiveness of the proposed method, especially with respect to a simple rule-based strategy.

Keywords: energy management, evolutionary algorithm, microgrid, sizing, unit commitment.

1 Nomenclature

2 Acronyms

3	BSS	battery storage systems
4	EA	evolutionary algorithms
5	EMS	energy management systems
6	ESS	energy storage system
7	FC	fuel cell
8	GA	genetic algorithm
9	HSS	hydrogen storage systems
10	LOH	level-of-hydrogen
11	LPSP	loss of power supply probability
12	MILP	mixed integer linear programming
13	PV	photovoltaic panels
14	RBS	rule-based strategies
15	RES	renewable energy sources
16	SOC	state-of-charge
17	UC	unit commitment

18 WT wind turbines

19 Symbols

20	α	penalty value for load shedding
21	β	penalty value for curtailed PV output
22	Δt	sampling time
23	η_{bat}	BSS charging efficiency
24	η_{PV}	PV panels efficiency
25	$\widetilde{P}_{load}(t)$	actual load in time t
26	$\widetilde{P}_{PV}(t)$	actual output of PV in time t
27	$B_{cost}^{ch}(t)$	BSS charging cost in time t
28	$B_{cost}^{dich}(t)$	BSS discharging cost in time t
29	C^{inv}	investment cost of components
30	C^{mnt}	annual maintenance costs of components
31	C_T	PV temperature coefficient
32	C_{cap}	capital cost of microgrid
33	C_{mnt}	annual maintenance cost of microgrid
34	C_{op}	operation cost
35	C_{bat}^{inv}	investment cost for the BSS
36	C_{ele}^{inv}	investment cost of the electrolyzer

*Corresponding author.

Email addresses: bei.li@utbm.fr (Bei Li), robin.roche@utbm.fr (Robin Roche), abdellatif.miraoui@utbm.fr (Abdellatif Miraoui)

37 $C_{ele}^{o\&m}$ operation and maintenance costs of the electrolyzer

38 C_{ele}^{start} startup cost of the electrolyzer

39 C_{fc}^{inv} investment cost of the FC

40 $C_{fc}^{o\&m}$ operation and maintenance costs of the FC

41 $C_{fc}^{o\&m}$ startup cost of the FC

42 CRF capital recovery factor

43 E_{OC} open-circuit voltage of one FC cell

44 Er_{load} error bound of load

45 Er_{PV} error bound of PV output

46 F Faraday constant

47 $F(.)$ total cost function

48 G_A global solar radiation

49 $H_{cost}^{ele}(t)$ utilization cost of the electrolyzer in time t

50 $H_{cost}^{fc}(t)$ utilization cost of the FC in time t

51 $I_{el}(t)$ current of the electrolyzer in time t

52 $I_{el}(t)/A_{el}$ current density of the electrolyzer

53 $i_{fc}(t)$ current density in one FC cell in time t

54 $N_{bat,cyc}$ number of cycles of the BSS

55 $N_{bat,hr}^{ele}$ operation hours of the electrolyzer over its lifetime

56 $N_{bat,hr}^{fc}$ operation hours of the FC over its lifetime

57 N_{el} number of electrolyzer cells

58 N_{fc} number of FC cells

59 n_{inv} expected life span of the microgrid

60 $P_{load}(t)$ forecasted load in time t

61 $P_{PV}(t)$ output power of PV panels in time t

62 P_{STC} PV array rated power

63 r real interest rate

64 T working temperature of the electrolyzer

65 T_C temperature of panels

66 T_{hor} time horizon

67 $V_{el}(t)$ voltage of the electrolyzer in time t

68 $V_{fc}(t)$ voltage of the FC in time t

69 V_{rev} reverse voltage of the electrolyzer

70 Variables

71 $\Delta\delta_{ele}$ status of the electrolyzer (starting or not)

72 $\Delta\delta_{fc}$ status of the FC (starting or not)

73 $\delta_{ele}(t)$ state (on or off) of the electrolyzer

74 $\delta_{fc}(t)$ state (on or off) of the FC

75 $\dot{n}_{el}^{H_2}(t)$ production rate of hydrogen of the electrolyzer in time t

76 $\dot{n}_{fc}^{H_2}(t)$ consumption rate of hydrogen of the FC in time t

77 C_{bat} capacity of the BSS

79 $LOH(t)$ state of hydrogen tanks in time t

80 N_{PV} number of PV panels

81 $P_{ch}(t)$ BSS charging power in time t

82 $P_{curt}(t)$ curtailed PV output in time t

83 $P_{disch}(t)$ BSS discharging power in time t

84 $P_{el}(t)$ input power of the electrolyzer in time t

85 P_{el}^{max} maximum input power of electrolyzer

86 $P_{fc}(t)$ output power of th FC in time t

87 P_{fc}^{max} maximum output power of fuel cell

88 $P_j(t)$ output power of unit j in time t

89 $P_{LS}(t)$ shed load in time t

90 $SOC(t)$ state of BSS in time t

91 $V_{H_2}^{max}$ maximum volume of hydrogen tanks

92 $Z_j(t)$ actual output power of unit j in time t

93 1. Introduction

94 In order to limit global warming and reduce fossil fuel con-
 95 sumption, renewable energy sources (RES) such as photo-
 96 voltaic panels (PV) and wind turbines (WT) are more and more
 97 commonly used to generate electricity. The integration of such
 98 intermittent sources is a challenge for grid operators, as the bal-
 99 ance between generation and demand must be met in real-time.
 100 This is especially a concern for small power systems such as
 101 microgrids, that can operate islanded, i.e., not connected to the
 102 main grid. Microgrids typically include distributed generation
 103 and storage [1, 2], and are increasingly found in remote areas
 104 [3, 4] or where power system resilience is a crucial concern
 105 [5, 6].

106 To enable RES integration, energy storage systems are con-
 107 sidered as a key solution, as they enable storing excess gener-
 108 ation for later use [7]. Battery storage systems (BSS) are typ-
 109 ically used for short-term storage [8], but seem inappropriate
 110 for long-term storage due to their low energy density and non-
 111 negligible self-discharge rate [9]. Hydrogen storage systems

(HSS), on the other hand, are used for long-term storage, such as seasonal storage. HSS combine an electrolyzer to produce hydrogen from electricity, an hydrogen storage tank and a fuel cell (FC) to produce electricity from hydrogen. [10] discusses FC systems, while [11] researches about the PV/FC hybrid systems. In [12], a Matlab/Simulink model is built to simulate a PV/FC hybrid energy system. [13] also builds a simulation model of another PV/FC/ultracapacitors stand-alone microgrid.

In this work, we focus on the optimal sizing of microgrids where PV panels are used as the primary energy source, and BSS and HSS are used as storage units (Fig. 2). Finding the optimal size for each of these components, i.e., finding the capacity or rated power for each component that ensures adequate supply at minimum cost, is a challenge because the sizing result is affected not only by the architecture of the system, but also by the adopted energy management strategy [14]. Depending on how components such as storage units are used, the necessary capacity may change significantly, which in turn impacts the size of other components as well as overall costs. Another aspect to consider is the impact of uncertainty on PV output and load. Forecasting errors change the input data profiles and lead to suboptimal scheduling results, which in turn influences sizing results. To address these challenges, this paper presents a leader-follower co-optimization method to size islanded microgrids, which also considers uncertainty on input data.

The optimal sizing problem is a non-convex and non-linear combinatorial optimization problem [15], and for the solution of this problem, various optimization methods have been presented in [16]. In [17], authors review 68 computer tools which can be used for analyzing RES integration, but the results show that there is no tool that can address all aspects of hybrid microgrid system. As the part of artificial intelligence, evolutionary algorithms (EA) are optimization algorithm which can be used to solve combinatorial and nonlinear optimization problems. For example, [18, 15] compare several EA for the optimal sizing of a hybrid system, where the objective function is the total annual cost. Other papers use various metaheuristics, [19] uses ant colony optimization (ACO) to get size values of PV/wind hybrid system. In [20], artificial bee swarm optimization (ABSO) used to solve the sizing problem of PV/WT/FC hybrid system considering loss of power supply probability (LPSP). Simulated annealing and tabu search (TS) are used in [3]. [21] studies the performance of different particle swarm optimization (PSO) algorithm variants to determine the size results of hybrid (PV/wind/Batt) system.

In most of these papers, a simple control strategy is selected when there is surplus power, the excess energy is stored in the ESS, and when there is a shortage of power, the ESS discharges or controllable generators (diesel gensets or FC) are turned on. Economic criteria are not considered in most cases. Some papers use more advanced strategies based on rules (rule-based strategies (RBS)) to control energy flows. Various algorithms are used, such as a multi-objective genetic algorithm (GA) [22], a hybrid GA [23], or an improved bat algorithm [24]. However, the limits of RBS are quickly reached when more than a few components are included in the system, as the number of required rules significantly increases. Moreover, these strate-

gies cannot provide optimal results regarding how the state-of-charge of storage units is controlled over time. More advanced energy management systems (EMS), that primarily focus on economic dispatch with EA, are also presented in the literature. [25] presents a decentralized energy management strategy based on multi-agent systems and fuzzy cognitive Maps. In [26], authors propose a non-cooperative game theory-based EMS. [27] proposes a bi-level optimization energy management approach of multiple microgrids. Economic dispatch is solved in each microgrid, and then a secondary-level optimization is used to seek the minimum operation cost for the set of microgrids. Multiperiod ABCO [28], multi-layer ACO [29], multiperiod gravitational search algorithm [30], and multi-period imperialist competition algorithm [31] are also used for economic dispatch applications. [32] presents an operational architecture for Real Time Operation (RTO) of an islanded microgrid. A limit of economic dispatch approaches for EMS is that set points are determined only based on current conditions, but future conditions are not considered.

An improved method for energy management, that can take into account multiple objectives and constraints, is thus required. Model-predictive control (MPC) offers a solution, and is commonly used in power systems in the form of unit commitment (UC). UC enables scheduling the use of multiple generation units over a given time horizon [33], for example over a day. It can also be extended to consider storage units and other devices. For example, in [9], the authors present a UC optimization method to economically schedule BSS and HSS. [34] studies the thermal power plant UC problem integrated with a large scale ESS. In [35], an integrated framework for a stand-alone microgrid with objectives of increasing stability and reliability and reducing costs is described. The UC method is used to determine generators outputs for the next day. [36] presents a two-stage planning and design method for microgrids. GA is used to solve the optimal design problem and a mixed integer linear programming (MILP) algorithm enables determining the optimal operation strategy. In [37], a mixed integer nonlinear programming (MINLP) approach for day-ahead scheduling a combined heat and power plant is proposed. Another MINLP-based EMS algorithm is presented in [38]. [39] describes an approach for security-constrained UC with integrated ESS and wind turbines. Overall, the above research papers show that the UC method is commonly used and adequate for scheduling the use of microgrid components, including energy storage units. However, contrary to works focusing on sizing that primarily focus on EA, papers on UC mainly use classical non-linear or linear programming techniques (MINLP or MILP) [40, 37].

A UC algorithm does however rely on forecast data to compute schedules. As forecasting errors are inevitable, the scheduling algorithm must consider these errors. In the case studied in this paper, errors on PV output and load impact schedules as well as sizing results. Two main approaches to consider forecasting uncertainty are found in the literature: scenario-based method [41, 42, 43] and robust optimization [44, 45, 46, 47]. [41] presents a stochastic method based on cloud theory to handle uncertainty, and uses a krill herd algorithm to solve the optimization problem. [42] describes

226 a stochastic optimization for microgrid energy and reserv^e282
 227 scheduling. Wind and PV generation fluctuations for each hour²⁸³
 228 are represented by 5-interval discrete probability distribution²⁸⁴
 229 functions. A scenario tree technique is then used to combin^e285
 230 different states of wind and PV fluctuations. [43] presents a²⁸⁶
 231 scenario-based robust energy management method. Taguchi^s287
 232 orthogonal array testing method is used to provide possible test²⁸⁸
 233 ing scenarios, and determine the worst-case scenario. At last²⁸⁹,
 234 the Monte Carlo method is used to verify the robustness of the²⁹⁰
 235 approach. In [44], uncertainty is quantified in terms of pre²⁹¹-
 236 diction intervals by a non-dominated sorting genetic algorithm²⁹²
 237 (NSGA-II) trained by a neural network. Robust optimization is²⁹³
 238 then used to seek the optimal solution to the problem. [45] uses²⁹⁴
 239 robust optimization-based scheduling for multiple microgrids²⁹⁵,
 240 considering uncertainty. The problem is transformed to a min²⁹⁶-
 241 max robust problem, and is then solved using linear duality the²⁹⁷-
 242 ory and the Karush-Kuhn-Tucker (KKT) optimality conditions²⁹⁸.
 243 [47] presents a robust EMS for microgrids. Authors use a fuzzy²⁹⁹
 244 prediction interval model to obtain the uncertainty boundary of³⁰⁰
 245 wind output, and then the upper and lower boundaries of wind³⁰¹
 246 energy are interpreted as the best and worst-case operating con³⁰²-
 247 ditions. In the above papers, scenario-based methods usually³⁰³
 248 require generating many scenarios, which can take a lot of time³⁰⁴
 249 to simulate. On the other hand, robust methods are used to find³⁰⁵
 250 the worst case, which requires less computation time, although³⁰⁶
 251 results are more conservative. As a consequence, in this paper³⁰⁷,
 252 a robust optimization method is selected to find the worst case³⁰⁸
 253 and best case based on the forecasting error.

254 The above review of the state-of-the-art has shown that a
 255 sizing methodology needs to use an appropriate energy man-
 256 agement or scheduling approach, and that MPC-based UC fits
 257 these needs. Several papers have considered such combina-
 258 tions of sizing and energy management algorithms. For exam-
 259 ple, [48] presents a co-optimization method to size stand-alone
 260 microgrids with two GA: one for the sizing, and another one
 261 for the scheduling. In [49], authors present a co-optimization
 262 method for microgrid planning in electrical power systems. The
 263 leader problem optimizes the planning decisions for the micro-
 264 grids and the main grid, and, with the proposed plan, the short-
 265 term and economic operation subproblems are solved to check
 266 whether constraints are met or not. In [50], authors also present
 267 a microgrid planning model. The problem is decomposed into
 268 an investment master problem and an operation subproblem.
 269 The two problems are linked via the benders decomposition
 270 method. Finally, in [51], the authors present a bi-level program
 271 for the sizing of islanded microgrids with an integrated com-
 272 pressed air energy storage (CAES). The upper level problem is
 273 solved using GA, and the lower level problem is solved using
 274 the MILP technique.

275 This paper introduces a general method to size a stand-alone
 276 microgrid (PV-BSS-HSS) considering technical and economic
 277 criteria, with a combination of EA and UC optimization. Com-
 278 pared to existing literature, contributions include:

- 279 1. A bi-level optimization method to perform microgrid siz³¹¹-
 280 ing. A genetic algorithm is used to compute the sizing of³¹²
 281 the components to minimize the total annual cost (capital,³¹³

maintenance and operation) of the system. Each candi-
 date solution (set of components sizes) is evaluated with
 a MILP UC algorithm. The design bi-level optimization
 framework is shown in Fig. 1.

2. The used UC optimization is used to control energy flows
 considers technical and economic criteria, such as the op-
 eration costs of the components, the startup costs of the
 fuel cell and the electrolyzer, the state-of-charge (SOC) of
 the BSS, the level-of-hydrogen (LOH) of hydrogen tanks.
 In addition to these, the load shedding and PV power cur-
 tailments resulting from sizing values are determined and
 used to evaluate candidate solutions.
3. A 1-hour resolution rolling-horizon simulation is used to
 verify the validity of the obtained sizing solutions, and to
 adjust the sizing values if required, especially as the sizing
 algorithm input data uses a 1-week resolution to improve
 computation speed.
4. Uncertainty on PV generation and load is taken into ac-
 count using a robust method. Sizing results are adjusted
 depending on forecasting errors.
5. The impact of different initial states for SOC and LOH and
 different penalty values for load shedding and power cur-
 tailments is assessed to determine the sensitivity of results
 with respect to these parameters.
6. Finally, results are compared with a rule-based strategy
 commonly used in the literature, in order to further evalu-
 ate the performance of the algorithm.

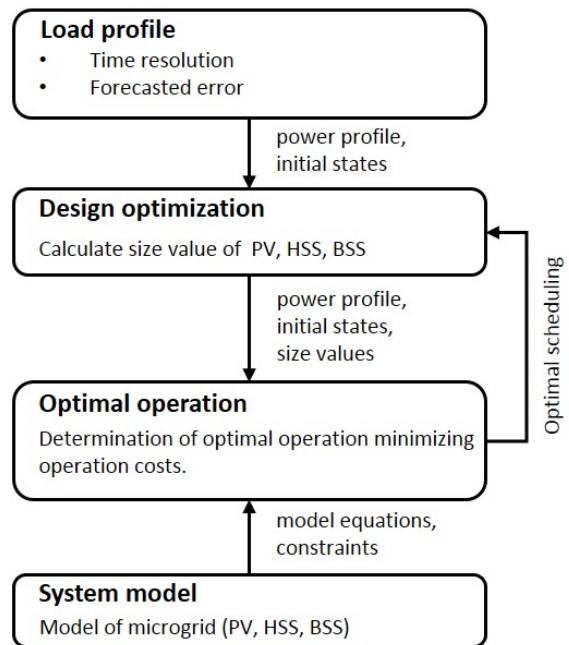


Figure 1: Bi-level optimization framework.

The rest of this paper is structured as follows. Section 2 in-
 troduces the system model. Section 3 describes the UC strategy
 and Section 4 the EA-based sizing problem formulation. Fi-
 nally, Section 5 presents the simulation results while Section 6
 concludes the paper.

2. System model

A stand-alone microgrid with four main components is considered (Fig. 2): PV panels, a BSS, an HSS (with an electrolyzer, hydrogen tanks and a fuel cell), and a load corresponding to a building. Static converters are not modeled, as their impact is negligible on sizing results.

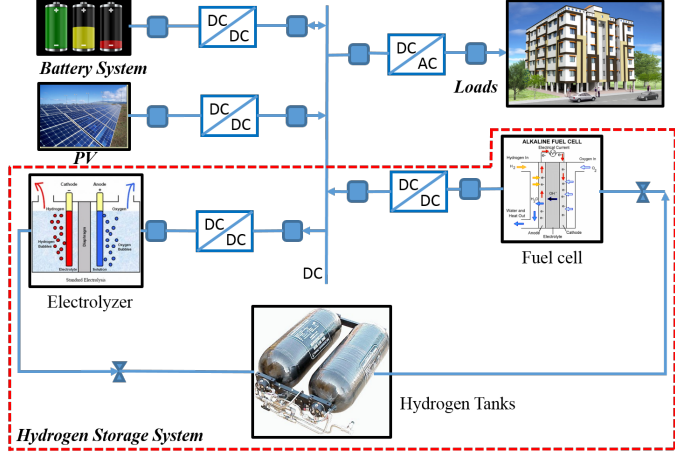


Figure 2: Microgrid architecture.

2.1. PV panels

The output of the PV panels is calculated using [52, 11]:

$$P_{PV}(t) = N_{PV} \cdot \eta_{PV} \cdot P_{STC} \cdot \frac{G_A(t)}{G_{STC}} \cdot (1 + (T_C(t) - T_{STC}) \cdot C_T) \quad (1)$$

where N_{PV} is the number of panels, η_{PV} is the panels efficiency, P_{STC} is the PV array rated power in W_p under standard test conditions (STC), G_A is the global solar radiation received by the panels in kW/m^2 , G_{STC} is the solar radiation under STC ($1 kW/m^2$), T_C is the temperature of the panels, T_{STC} is the STC temperature, and C_T is the PV temperature coefficient.

2.2. Battery

The state of the BSS is represented by its state-of-charge:

$$SOC(t) = SOC(t - \Delta t) + \frac{\eta_b \cdot P_{ch}(t) \cdot \Delta t}{C_{bat}} - \frac{P_{disch}(t) \cdot \Delta t}{C_{bat}} \quad (2)$$

where η_{bat} is the charging efficiency, $P_{ch}(t)$ is charging power, $P_{disch}(t)$ is the discharging power, Δt is the sampling time, and C_{bat} is the capacity of the battery pack.

2.3. Electrolyzer

Electrolyzers are used to produce hydrogen (H_2) from electricity. The characteristic of the electrolyzer can be described as follows [53, 54]:

$$V_{el}(t) = N_{el} \cdot V_{rev} + (r_1 + r_2 \cdot T) \cdot \frac{I_{el}(t)}{A_{el}} + (s_1 + s_2 \cdot T + s_3 \cdot T^2) \times \log \left(1 + \left(t_1 + \frac{t_2}{T} + \frac{t_3}{T^2} \right) \cdot \frac{I_{el}(t)}{A_{el}} \right) \quad (3)$$

where $V_{el}(t)$ is the voltage of the electrolyzer, N_{el} is the number of cells, V_{rev} is the reversible cell potential, T is the working temperature (assumed constant), and $I_{el}(t)/A_{el}$ (in A/m^2 , with A_{el} the area) is the current density. Variables $r_1, r_2, s_1, s_2, s_3, t_1, t_2, t_3$ are empirical constant coefficients.

The production rate of hydrogen of the electrolyzer is then given by Faraday's law:

$$\dot{n}_{el}^{H_2}(t) = \eta_F(t) \cdot \frac{N_{el} I_{el}(t)}{2F} \quad (4)$$

where F is the Faraday constant, and I_{el} is the current in the electrolyzer. η_F is Faraday's efficiency, which provides a relation between the actual production rate of hydrogen and its theoretical value, namely:

$$\eta_F(t) = \frac{(I_{el}(t)/A_{el})^2}{f_1 + (I_{el}(t)/A_{el})^2} f_2 \quad (5)$$

where f_1 and f_2 are empirical coefficients.

Using the above equations, an equation relating $P_{el}(t)$ and $\dot{n}_{el}^{H_2}(t)$ is obtained, in the form of:

$$P_{el}(t) = f(\dot{n}_{el}^{H_2}(t)) \quad (6)$$

where $f(\cdot)$ is a nonlinear function. Due to constraints described in Section 3, this function is linearized, such that:

$$P_{el}(t) = k_{el} \cdot \dot{n}_{el}^{H_2}(t) \quad (7)$$

where k_{el} is a constant. The linearization is done via a linear regression on the curve obtained from (6). The maximum value of P_{el} is noted P_{el}^{max} .

2.4. Fuel cell

Fuel cells consume H_2 and oxygen to produce electricity and water [10, 11, 12, 55]. A simple electrical model is used to describe the characteristic voltage curve of the FC [55]:

$$V_{fc}(t) = (E_{OC} - r_{fc} \cdot i_{fc}(t) - a \cdot \ln(i_{fc}(t)) - m \cdot e^{s \cdot i_{fc}(t)}) \cdot N_{fc} \quad (8)$$

where V_{fc} is the voltage of the FC, E_{OC} is the open-circuit voltage of one cell, $i_{fc}(t)$ is the current density in one cell, N_{fc} is the number of cells, and $r_{fc}, s, a,$ and m are empirical coefficients.

The hydrogen consumption of the FC depends on its current and is given by:

$$\dot{n}_{fc}^{H_2}(t) = \frac{N_{fc} I_{fc}(t)}{2FU} \quad (9)$$

where U is the utilization efficiency of hydrogen by the fuel cell.

As for the electrolyzer, the model is linearized to obtain:

$$P_{fc}(t) = k_{fc} \cdot \dot{n}_{fc}^{H_2}(t) \quad (10)$$

where k_{fc} is a constant. The maximum value of P_{fc} is noted P_{fc}^{max} .

349 2.5. Hydrogen tank

Hydrogen tanks are used to store the hydrogen produced by the electrolyzer. The stored hydrogen is then supplied to the FC to generate electricity. Similarly to the BSS, a quantity named level of hydrogen (LOH) is used to represent the state of the tank:

$$LOH(t) = LOH(t - \Delta t) + \dot{n}_{el}^{H_2}(t) \cdot \Delta t - \dot{n}_{fc}^{H_2}(t) \cdot \Delta t \quad (11)$$

350 Then, using the ideal gas law ($PV = nRT$), the volume of the
351 tank V_{H_2} can easily be determined.

352 3. Scheduling strategy

353 As the results of the sizing process depend on how the differ-
354 ent components are used (i.e., what is their output), an appro-
355 priate control strategy is required. Contrary to classical compo-
356 nents, ESS introduce a temporal link between time steps and
357 scheduling algorithms have to consider this link to ensure that
358 the SOC remains within allowed bounds. This constraint is nec-
359 essary to ensure that the results of the sizing are adequate, and
360 components oversizing is avoided. As a consequence, it is nec-
361 essary to predict the evolution of the entire system, including
362 the PV generation which is the primary source of energy for the
363 microgrid.

364 This paper uses a form of MPC to plan the operation of the
365 system in advance, using forecasts. This MPC strategy is a UC
366 algorithm. Due to the presence of mixed logical and integer
367 variables, the problem is expressed as a MILP problem.

368 3.1. Cost function

In order to achieve economically efficient operation, the uti-
lization cost of the BSS and the HSS need to be quantified and
minimized over a given time horizon [9, 56, 48]. For the BSS,
aging is a major concern that limits the lifetime of the device.
As a consequence, the investment cost and the degradation of
the BSS have to be taken into account in the operation cost. The
utilization cost for charge and discharge are then implemented
as follows [56]:

$$B_{cost}^{ch}(t) = \frac{C_{bat}^{inv} \cdot P_{ch}(t) \cdot \eta_b}{2 \cdot N_{bat,cyc}} \quad (12)$$

$$B_{cost}^{disch}(t) = \frac{C_{bat}^{inv} \cdot P_{disch}(t)}{2 \cdot N_{bat,cyc}} \quad (13)$$

369 where C_{bat}^{inv} is the investment cost for the BSS, and $N_{bat,cyc}$ the
370 number of cycles over its lifetime.

For the HSS, the O&M and the startup costs must also be
considered. The utilization cost of the electrolyzer and the FC
can be computed as follows [56]:

$$H_{cost}^{ele}(t) = \left(\frac{C_{ele}^{inv}}{N_{bat,hr}^{ele}} + C_{ele}^{o\&m} \right) \cdot \delta_{ele}(t) + C_{ele}^{start} \cdot \Delta \delta_{ele}(t) \quad (14)$$

$$H_{cost}^{fc}(t) = \left(\frac{C_{fc}^{inv}}{N_{bat,hr}^{fc}} + C_{fc}^{o\&m} \right) \cdot \delta_{fc}(t) + C_{fc}^{start} \cdot \Delta \delta_{fc}(t) \quad (15)$$

where C_{ele}^{inv} and C_{fc}^{inv} are the investment costs for the electrolyzer
and the FC. $C_{ele}^{o\&m}$ and $C_{fc}^{o\&m}$ are the operation and maintenance
costs of both components. Similarly, C_{ele}^{start} and C_{fc}^{start} are their
startup cost. $N_{bat,hr}$ represents the number of hours of operation
of the HSS over its lifetime. $\delta_{ele}(t)$ and $\delta_{fc}(t)$ describe their state
(i.e., 1 for on, 0 for off). Finally, $\Delta \delta_i$ represents whether the unit
is starting or not, and is defined as:

$$\Delta \delta_i(t) = \max\{\delta_i(t) - \delta_i(t-1), 0\}, i = \{ele, fc\} \quad (16)$$

Based on the previous cost functions, the total operation cost
function for the entire microgrid, over a time horizon of T_{hor}
steps, can be built:

$$C_{op} = \sum_{t=1}^{T_{hor}} \left(B_{cost}^{ch}(t) + B_{cost}^{dis}(t) + H_{cost}^{ele}(t) + H_{cost}^{fc}(t) \right) \quad (17)$$

$$+ \alpha \cdot P_{LS}(t) + \beta \cdot P_{curt}(t)$$

where $P_{LS}(t)$ is the shed load, $P_{curt}(t)$ is the curtailed PV output,
and α and β are the corresponding penalty values. Load shed-
ding (LS) and PV curtailment (PVC) are two means of flexibil-
ity to ensure a balance between generation and demand. How-
ever, their use has to be minimized due to their impact on cus-
tomer comfort and system efficiency, respectively. The values
of penalty coefficients α and β are thus chosen to discourage the
use of LS and PVC. A form of demand response could however
also be used [57, 58], but is kept for future work.

380 3.2. Constraints

The operation of the various components is subject to several
constraints, as is the islanded operation of the system. In the
following equations, $i = \{ele, fc\}$ and $j = \{ele, fc, ch, disch\}$.
First, all component outputs have to be between their minimum
and maximum values:

$$P_j^{min} \leq P_j(t) \leq P_j^{max} \quad (18)$$

In order to consider the status of each device (on or off), the
above equation becomes:

$$\delta_j(t) \cdot P_j^{min} \leq Z_j(t) = \delta_j(t) \cdot P_j(t) \leq \delta_j(t) \cdot P_j^{max} \quad (19)$$

Due to linearity constraints, this equation can then in turn be
transformed into the following two inequalities:

$$Z_j(t) \leq P_j(t) - (1 - \delta_j(t)) \cdot P_j^{min} \quad (20)$$

$$Z_j(t) \geq P_j(t) - (1 - \delta_j(t)) \cdot P_j^{max}$$

Another constraint is that the electrolyzer and the FC should
not be working at the same time, i.e., the HSS is either charging
or discharging:

$$\delta_{ele}(t) + \delta_{fc}(t) \leq 1 \quad (21)$$

A similar constraint is used for the BSS:

$$\delta_{ch}(t) + \delta_{disch}(t) \leq 1 \quad (22)$$

The SOC and LOH constraints also have to be verified:

$$SOC_{min} \leq SOC(t) \leq SOC_{max} \quad (23)$$

$$V_{H_2}^{min} \leq V_{H_2}(t) \leq V_{H_2}^{max} \quad (24)$$

Then, equation (16) can be rewritten as:

$$\Delta\delta_i(t) = \delta_i(t) \cdot (1 - \delta_i(t-1)), i = \{ele, fc\} \quad (25)$$

From [59], the above nonlinear equation can be transformed into the following linear constraints:

$$-\delta_i(t) + \Delta\delta_i(t) \leq 0 \quad (26)$$

$$-(1 - \delta_i(t-1)) + \Delta\delta_i(t) \leq 0 \quad (27)$$

$$\delta_i(t) + (1 - \delta_i(t-1)) - \Delta\delta_i(t) \leq 1 \quad (28)$$

Finally, as the system is islanded, the balance between generation and demand has to be met at all time steps, so:

$$\begin{aligned} P_{PV}(t) - P_{curt}(t) - (P_{load}(t) - P_{LS}(t)) \\ = Z_{ele}(t) - Z_{fc}(t) + Z_{ch}(t) - Z_{dis}(t) \end{aligned} \quad (29)$$

3.3. Problem formulation

Using the above cost function and constraints, the microgrid UC problem can be summarized as follows, where \bar{S} is the set of variables:

$$\min_{\bar{S}} \{C_{op}\} \quad \text{s.t.} \quad (2), (7), (10), (11), (18) - (29) \quad (30)$$

4. Sizing algorithm

The scheduling strategy presented in the previous section requires several input variables. Some of these variables correspond to the maximum rating or capacity of each component, what are the results of the sizing algorithm. Other inputs are parameters set by the user, such as the initial SOC and LOH values, and the penalty coefficients α and β . The impact of these parameters on results will be discussed in Section 5.

4.1. Leader-follower structure

The sizing problem aims at finding the optimal size of the PV, BSS, electrolyzer and FC components to achieve the most cost-effective solution over a given time period. Let $N_{PV} \in \mathbf{N}_{PV}$, $C_{bat} \in \mathbf{C}_{bat}$, $V_{H_2}^{max} \in \mathbf{V}_{H_2}$, $P_{el}^{max} \in \mathbf{P}_{el}$, $P_{fc}^{max} \in \mathbf{P}_{fc}$. Set \mathbf{U} represent the whole set, namely, $\mathbf{U} = \mathbf{N}_{PV} \cup \mathbf{C}_{bat} \cup \mathbf{V}_{H_2} \cup \mathbf{P}_{el} \cup \mathbf{P}_{fc}$, and $U \in \mathbf{U}$.

The problem can then be formulated as a leader-follower problem [60]. The leader problem (the sizing problem) is as follows:

$$\min_{U \in \mathbf{U}} \{F(\mathbf{U})\} \quad (31)$$

where $F(\cdot)$ is a function representing the total cost of the system over the simulation duration.

The follower problem (the scheduling problem), is defined as:

$$\min_{U^*, \bar{S}} \{C_{op}\} \quad \text{s.t.} \quad (2), (7), (10), (11), (18) - (29) \quad (32)$$

where U^* is the set of sizing values obtained from the leader.

In other words, the leader first returns a candidate set of values for N_{PV} , C_{bat} , $V_{H_2}^{max}$, P_{el}^{max} , and P_{fc}^{max} . Then the follower uses these values to calculate the total operation cost using the algorithm described in Section 3. Based on this cost information, the leader adjusts the sizing values until an optimal value that minimizes the overall cost is found.

4.2. Leader problem objective function

To obtain a valid estimate of the actual cost of the system, operation cost is insufficient as capital and maintenance costs must also be considered [15, 48, 18]. In order to convert the initial capital cost to an annual capital cost, the capital recovery factor (CRF) is used [15]:

$$CRF = \frac{r(1+r)^{n_{inv}}}{(1+r)^{n_{inv}} - 1} \quad (33)$$

where r is the real interest rate and n_{inv} is the expected life span of the microgrid.

The total capital cost corresponds to the cost of buying the equipment, given by:

$$\begin{aligned} C_{cap} = CRF \cdot (N_{PV} \cdot C_{PV}^{inv} + P_{fc}^{max} \cdot C_{fc}^{inv} + P_{el}^{max} \cdot C_{ele}^{inv} \\ + V_{H_2} \cdot C_{tank}^{inv} + C_{bat} \cdot C_{bat}^{inv}) \end{aligned} \quad (34)$$

where C^{inv} variables represent the prices of the PV, FC, electrolyzer, hydrogen tanks and battery components.

Similarly, the annual maintenance cost is given by:

$$C_{mnt} = N_{PV} \cdot C_{PV}^{mnt} + V_{H_2} \cdot C_{tank}^{mnt} + C_{bat} \cdot C_{bat}^{mnt} \quad (35)$$

where C^{mnt} variables represent the annual maintenance costs of the PV, hydrogen tanks and battery components. As the O&M cost of the FC and the electrolyzer are considered in the operation strategy equations (12) to (15), they are not included in the annual cost.

The fitness function of the leader problem is thus the total cost function $F(\cdot)$ given by:

$$F = C_{cap} + C_{op} + C_{mnt} \quad (36)$$

Finally, the overall problem can be formulated as:

$$\begin{aligned} \min_{U \in \mathbf{U}} \{C_{cap} + \min_{U^*, \bar{S}} \{C_{op}\} + C_{mnt}\} \\ \text{s.t.} \quad (2), (7), (10), (11), (18) - (29) \end{aligned} \quad (37)$$

4.3. Simulation process

In order to obtain the optimal sizing for the system, the MILP-based scheduling algorithm and the EA-based sizing algorithm are combined.

A GA [23, 61] is used to solve the leader problem. GA are based on the natural selection process similar to biological evolution. Operators such as mutations, crossover and selection enable generating candidate solutions. The decision variables of the GA are rounded to the nearest higher value for use in the UC MILP algorithm.

The simulation process is shown in Fig. 3:

1. The population of N candidate solutions for the GA is randomly initialized.
2. Each of these solutions is then used with the follower problem. The UC MILP optimization is run. If the solution is infeasible, a new candidate solution is generated.
3. The GA fitness function value is then computed to determine the total cost of each candidate solution.
4. The process continues until any stopping criterion is met. An adaptive method is selected. Firstly, if the fitness function values for two consecutive steps are the same, then counter Num is incremented. If Num exceeds a given maximum value (here $Num^{max} = 50$), the simulation stops as the fitness function is not improving anymore. The second criterion is on the number of iterations, for which a maximum number (here $Gen^{max} = 200$) is set.

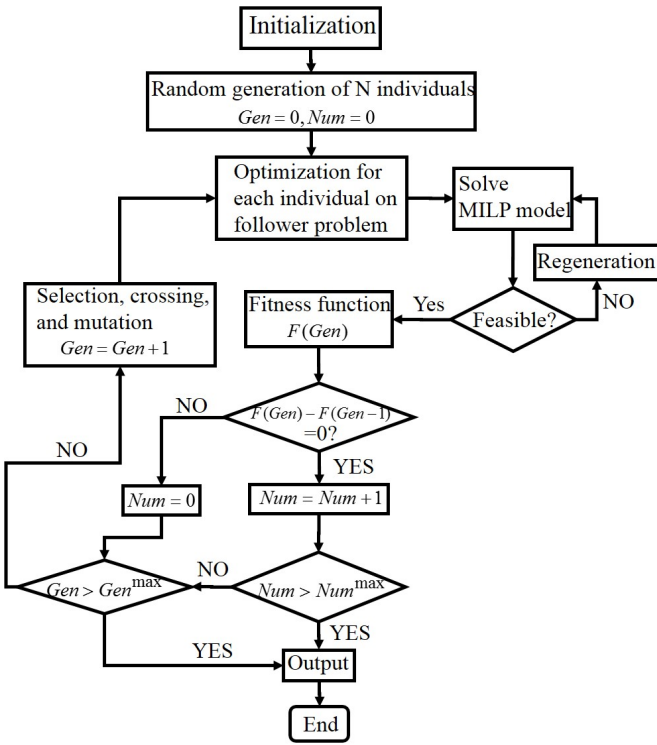


Figure 3: Optimization process outline.

5. Simulation results

In order to validate the sizing methodology, we run several simulation cases.

5.1. Simulation setup

Simulations are performed using Matlab R2014a and Gurobi 6.5.1, running on a desktop computer with an Intel Xeon 3.1 GHz processor, 16 GB RAM, and Microsoft Windows 7. Input data profiles for solar radiation and load (Fig. 4) are obtained and adapted from a research building located on the UTBM campus in Belfort, France. In order to analyze the sensitivity of sizing results to load levels, we use two load profiles.

As shown in Fig. 4, load profile 2 is 50% larger than load profile 1. Component parameters used in the simulations are given in Table 1.

In order to keep simulation time to reasonable durations, weekly average data is used for the input data. The approximate duration for each run is then of approximately 30 minutes. Although resolutions of 1 hour or more could be used, simulation durations would increase significantly and could not be performed on a regular computer.

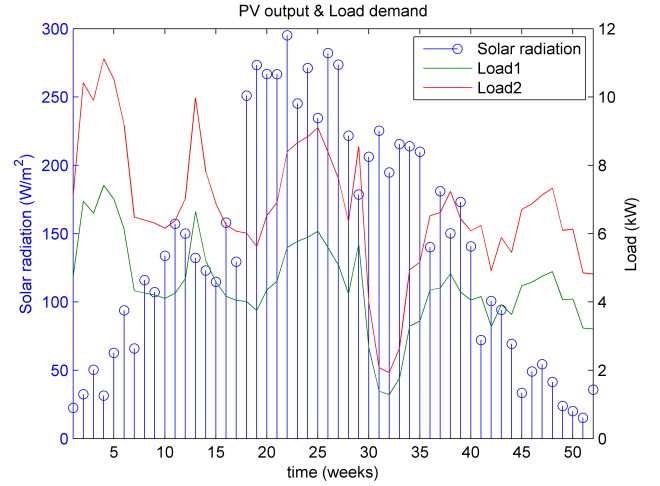


Figure 4: Weekly average solar radiation and load profiles.

5.2. Cases overview

To evaluate the impact of initial conditions and parameters, five cases are compared. Each case assumes different values for SOC_{ini} , LOH_{ini} , α and β , and one of the two load profiles. Case assumptions are summarized in Table 2. Cases 1A and 1B, and Cases 2A and 2B are designed to compare the influence of different initial states for SOC and LOH on the sizing results. Case 2 is also used to analyze the influence of different load levels on the sizing of the HSS and the BSS. Case 3 is designed to analyze the influence of the penalty values (α and β) on sizing results, with values ranging from 10^5 to 10^1 . Results are summarized in Table 3.

5.3. Results for Case 1

For Case 1A, the sizing results return 52 PV panels, a 6 kW FC, a 7 kW electrolyzer, tanks with a capacity of 7178 Nm^3 , and 189 kWh of batteries, for a total cost of €201,970. Here, unit Nm^3 corresponds to the volume under normal conditions (1 bar, 0°C). Based on the ideal gas law, we can estimate the volume for a higher pressure and temperature. For example, under 700 bar/15°C, the above volume would amount to 10.82 m^3 . Convergence results of the GA are shown in Fig. 5, and indicate that 200 generations seem sufficient. Similar convergence results are obtained for other cases.

Fig. 6 shows the scheduling results. The HSS is more frequently used than the BSS, as the HSS is cheaper to use when the power gap between PV output and load demand is large.

Table 1: Component and simulation parameters.

Fuel cell [10, 11, 12, 55, 48]	
A	0.03
r_{fc}	2.45×10^{-4}
m	2.11×10^{-5}
n	0.008
C_{fc}^{inv}	4,000 €/kW
$C_{fc}^{o\&m}$	0.2 €/h
Life cycles	30,000h
p_{fc}^{min}	1kW
Electrolyzer [53, 54, 48]	
r_1	0.0015
r_2	-6.019×10^{-6}
s_1	2.427
s_2	-0.0307
s_3	3.9×10^{-4}
t_1	0.214
t_2	-9.87
t_3	119.1
f_1	150
f_2	0.99
C_{ele}^{inv}	3,200 €/kW
$C_{ele}^{o\&m}$	0.2 €/h
Life cycles	30,000h
p_{ele}^{min}	1kW
Battery [48]	
C_{bat}^{inv}	470 €/kWh
C_{bat}^{mt}	1 €/kW.year
$N_{bat,cyc}$	2,000
SOC_{min}	0.5
SOC_{max}	0.9
Hydrogen tanks [48]	
C_{tank}^{inv}	150 €/Nm ³
C_{tank}^{mt}	10 €/Nm ³ .year
$V_{H_2}^{min}$	1Nm ³
PV panels[48]	
C_{pv}^{inv}	7,400 €/kW
C_{pv}^{mt}	6 €/kW.year
CRF [48]	
n_{inv}	20 years
r	0.05

Table 2: Simulation cases assumptions.

Cases	1A	1B	2A	2B	3
SOC_{ini}	0.5	0.9	0.5	0.9	0.5
LOH_{ini}	5000	3000	8000	7000	5000
α	10^5	10^5	10^5	10^5	10^3
β	10^5	10^5	10^5	10^5	10^3
Load profile	1	1	2	2	1

491 Fig. 7 shows the change in hydrogen level in the tanks. As in
 492 winter the PV output is insufficient, the HSS discharges mostly
 493 to supply the load, but in summer, PV output is large enough
 494 to enable the HSS to recharge and store hydrogen. Due to the

495 large penalty values (10^5) for LS and PVC, these two options
 496 are almost not used.

497 Fig. 7 also shows the SOC profile of the BSS, that is used
 498 as an auxiliary storage system to ensure the balance between
 499 generation and demand, while avoiding load shedding and PV
 500 curtailment.

501 For Case 1B, the initial SOC is larger and the initial LOH
 502 lower. The capacity of the hydrogen tank decreases to 5283
 503 Nm³, while the battery capacity decreases to 179 kWh. Conse-
 504 quently, the total cost also decreases to € 160,070. The schedul-
 505 ing results for Case 1B are similar to the ones obtained for Case
 506 1A, and are thus not shown. Fig. 8 shows the LOH and SOC
 507 levels. As the initial SOC is larger than for 1A, the total re-
 508 quired capacity is lower. For the LOH, the profile is almost the
 509 same as in Case 1A. For the SOC, in Case 1A, the initial state
 510 is the minimum SOC, so the BSS cannot discharge at the be-
 511 ginning, but for Case 1B, the initial state is the maximum SOC
 512 and the BSS can then discharge.

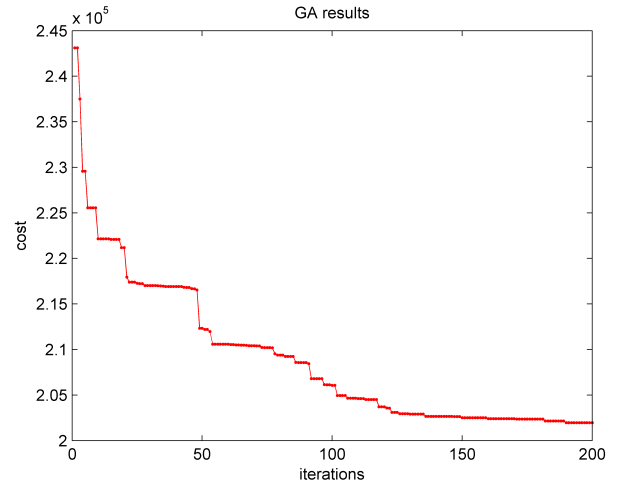


Figure 5: Comparison of the convergence of all three EA for Case 1A.

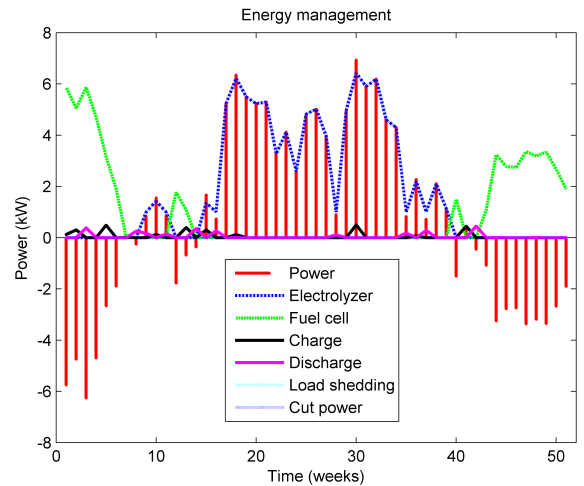


Figure 6: Scheduling results for case 1A. The curve labelled 'Power' corre-
 sponds to the PV output minus the load.

Table 3: Sizing results.

Case	Load	SOC_i	LOH_i	Total Cost [€]	C_{op} [€]	C_{cap} [€]	N_{PV}	P_{fc}^{max} [kW]	P_{el}^{max} [kW]	V_{H_2} [N.m ³]	C_{bat} [kWh]
1A	1	0.5	5000	201970	1697.8	127980	52	6	7	7178	189
1B	1	0.9	3000	160070	1663.2	105070	52	6	7	5283	179
2A	2	0.5	8000	219410	1725.1	137210	50	11	6	8000	158
2B	2	0.9	7000	200290	1674.5	128090	54	10	7	7000	190
3	1	0.5	5000	205160	4562.2	125120	52	7	7	7515	2
RBS	1	0.5	5000	276560	151.9	174640	57	7	8	10100	407

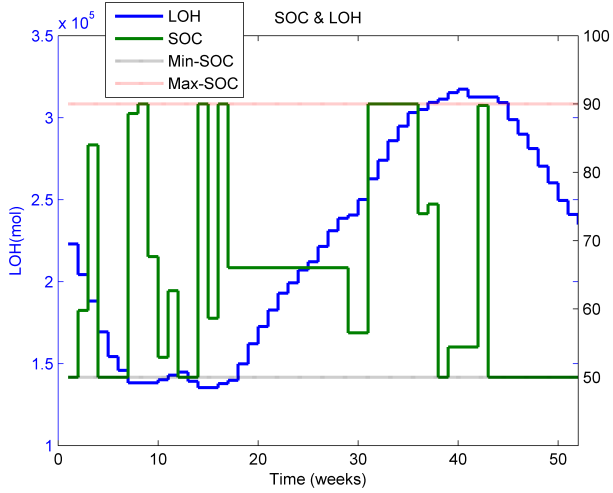


Figure 7: LOH and SOC for Case 1A.

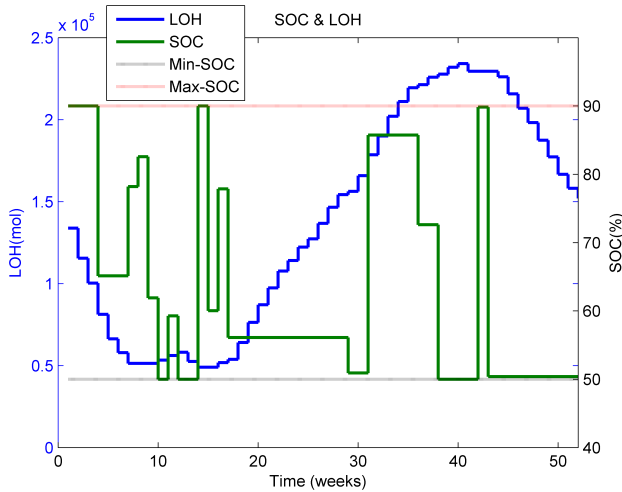


Figure 8: LOH and SOC for Case 1B.

519 the LOH and SOC profiles. The HSS is sufficient to provide
 520 energy to the load, especially at the beginning, so the needed
 521 battery capacity is lower. However, in Case 2B, the HSS is
 522 insufficient to meet the load, so more PV panels and battery
 523 energy are needed. We can also see that the rating of the FC
 524 is larger than in Case 1. As more energy is needed, it becomes
 525 cheaper to use the FC than the battery, hence the higher FC
 526 rating.

527 For Case 2B, the sizing results return 54 PV panels, a 10 kW
 528 FC, a 7 kW electrolyzer, tanks with a capacity of 7000 Nm³,
 529 and 190 kWh of batteries, for a total cost of € 200,290. As the
 530 load is higher than that of Case 1, more storage, in the form
 531 of BSS and HSS is needed. As the cost of the energy initially
 532 contained in the storage units is not accounted for, the algorithm
 533 increases the size of the storage units rather than increasing the
 534 number of PV panels. The obtained scheduling results are close
 535 to the ones shown in Fig. 9. Fig. 11 shows the LOH and SOC
 536 profiles. Due to slight differences in the scheduling results, the
 537 SOC curve is difference from the one in Case 2A. However, the
 538 curves for LOH is similar, as the HSS operates as a longer term
 539 storage unit.

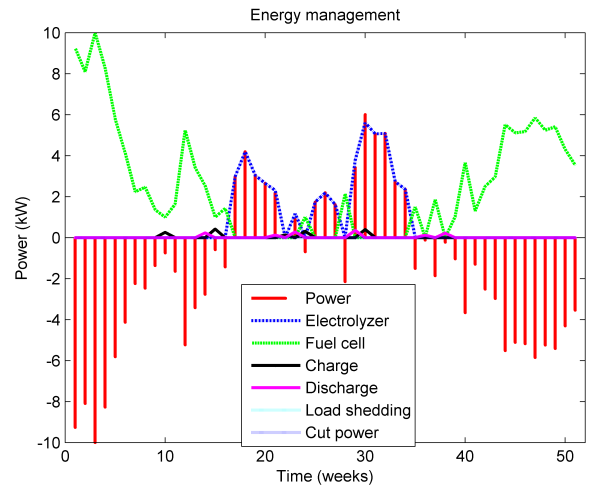


Figure 9: Scheduling results for Case 2A. The curve labelled 'Power' corresponds to the PV output minus the load.

513 5.4. Results for Case 2

514 For Cases 2A and 2B, the second load profile with a 50%
 515 higher demand is used. For Case 2A, the sizing results return
 516 50 PV panels, a 11 kW FC, a 6 kW electrolyzer, tanks with a
 517 capacity of 8000 Nm³, and 158 kWh of batteries, for a total cost⁵⁴¹
 518 of € 219,410. Fig. 9 shows the scheduling results, and Fig. 10⁵⁴²

5.5. Results for Case 3

In this case, as the penalty values are lower (10³ instead of
 10⁵), more energy is shed or curtailed. As a consequence, the

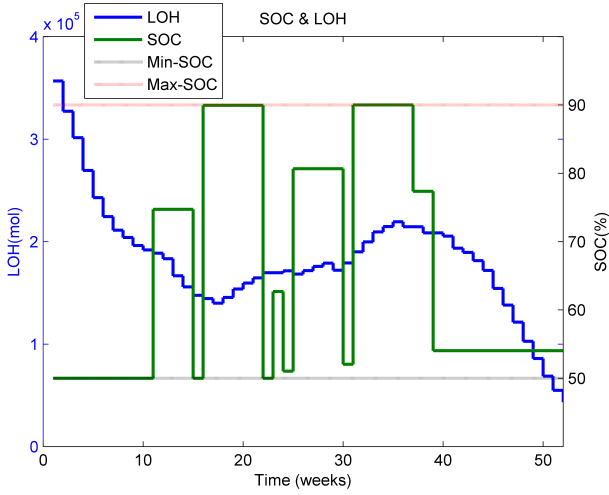


Figure 10: LOH and SOC for Case 2A.

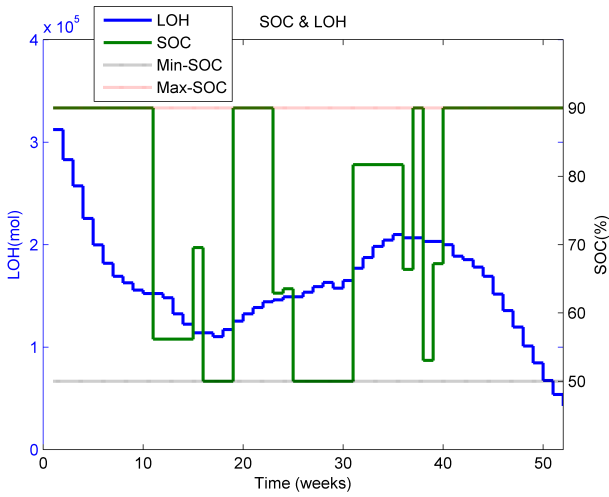


Figure 11: LOH and SOC for Case 2B.

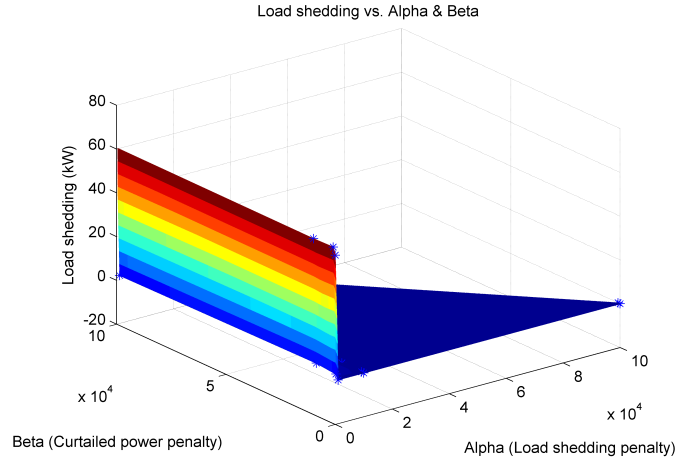


Figure 12: Load shedding vs. α & β .

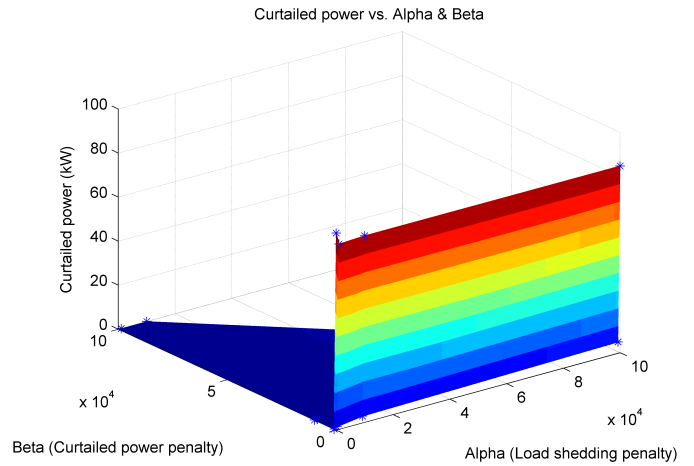


Figure 13: Curtailed power vs. α & β .

543 sizing results return 52 PV panels, a 7 kW FC, a 7 kW electro-
 544 lyzer, tanks with a capacity of 7515 Nm³, and 2 kWh of batteries,
 545 for a total cost of € 205,160. Detailed LS, PVC, LOH
 546 and SOC profiles are shown in Fig. 15.

547 The size of the battery is significantly smaller than in other
 548 cases. This can be explained by the lower values of the penalties
 549 for LS and PVC, which make these two options more competi-
 550 tive compared to using the BSS. In order to further evaluate the
 551 influence of the different penalty values, we simulate different
 552 combinations of α and β with Case 1A. The results are shown
 553 in Table 4 and Figs. 12 and 13, and indicate that the smaller
 554 the values of α and β , the larger the magnitude of LS and PVC,
 555 respectively.

556 Scheduling results are shown in Fig. 14, where we observe
 557 that limited LS and PVC occur, although for Cases 1 and 2
 558 the BSS was used to supply the load (due to its cheaper cost).
 559 As expected, the algorithm chooses the most economical way to
 560 operate the system.

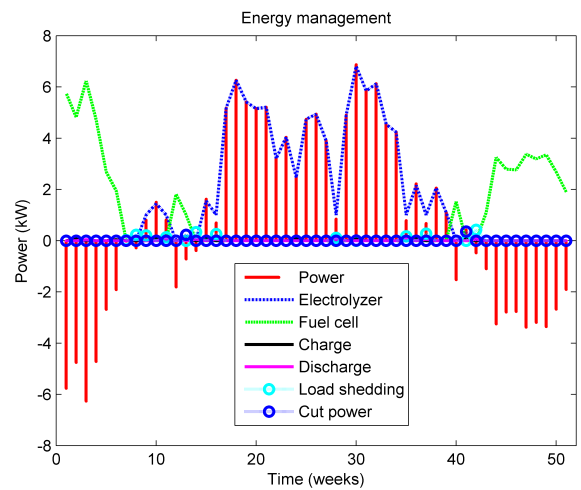


Figure 14: Scheduling results for Case 3. The curve labelled 'Power' corresponds to the PV output minus the load

Table 4: Sizing results with different penalty values for Case 1A.

Case 3	$\sum_{t=1}^{T_{hor}} P_{LS}(t)$ [kW]	$\sum_{t=1}^{T_{hor}} P_{curt}(t)$ [kW]	N_{PV}	P_{fc}^{max} [kW]	P_{el}^{max} [kW]	V_{H_2} [N.m ³]	C_{bat} [kWh]
$\alpha = 10^5, \beta = 10^3$	0	4.4576	51	7	7	6823	58
$\alpha = 10^5, \beta = 10^1$	0	84.8847	50	7	1	5026	2
$\alpha = 10^4, \beta = 10^1$	0	84.7377	50	7	2	5543	2
$\alpha = 10^4, \beta = 10^3$	0.0839	2.4054	55	7	8	8341	2
$\alpha = 10^4, \beta = 10^4$	0.0352	0	52	6	7	7601	170
$\alpha = 10^4, \beta = 10^5$	0.1297	0	59	7	8	11123	113
$\alpha = 10^3, \beta = 10^1$	0	84.1643	50	7	2	7015	2
$\alpha = 10^3, \beta = 10^3$	2.209	0.7691	52	7	7	7515	2
$\alpha = 10^3, \beta = 10^4$	3.0844	0	52	7	8	10978	11
$\alpha = 10^3, \beta = 10^5$	1.9553	0	54	7	8	8315	38
$\alpha = 10^1, \beta = 10^1$	57.3662	89.4729	50	2	2	5793	2
$\alpha = 10^1, \beta = 10^3$	60.5996	0	50	2	7	9110	1
$\alpha = 10^1, \beta = 10^4$	60.3302	0	50	2	7	9023	2
$\alpha = 10^1, \beta = 10^5$	60.5804	0	50	2	7	9157	2

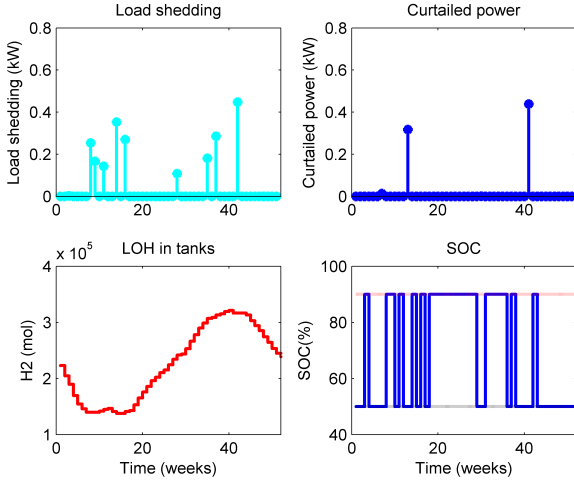


Figure 15: Shed and curtailed power, LOH and SOC profiles for Case 3.

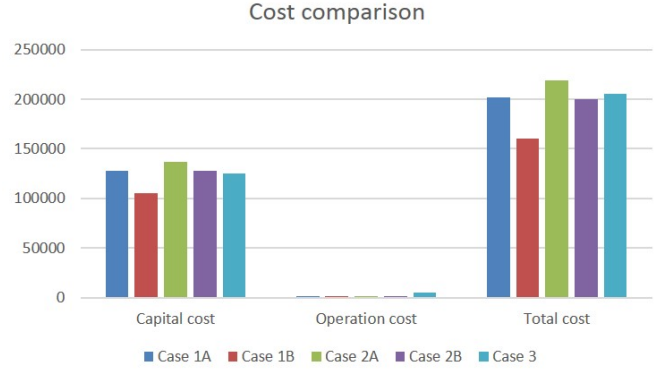


Figure 16: Comparison of costs for all cases.

5.6. Discussion of Cases 1 to 3

From the summary of results shown in Table 3, it can be observed that the sizing results and the total cost are impacted by the use of different input data and initial states. A comparison of the breakdown of costs for all cases is shown in Fig. 16. Results indicate that the capital costs are the highest, while O&M costs remain relatively small. As the only primary energy source is PV, these results are not surprising. The initial energy contained in the BSS and the HSS is however not considered. Case 3 has the largest O&M cost, due to the penalty values combined to LS and PVC. For Case 2A, more fuel cell and hydrogen tanks are needed, which results in the largest capital and total cost.

Simulations also show that the HSS is more appropriate for long term (seasonal) storage, as expected. This is especially valid as FC and electrolyzers have limited dynamics, and require BSS or other fast dynamics storage units to complement them and act as an auxiliary unit. On the other hand, because the discharge and charge power of the HSS are separate, the

degradation of the HSS will be slower than for the BSS.

Regarding LS and PVC penalty values, results have shown that values in the range of value $[10^3, 10^5]$ are reasonable and enable limiting the use of LS and PVC only to necessary cases. Values larger than 10^5 result in no LS or PVC at all, which can be problematic as they can be seen as flexibility means of last resort.

5.7. Comparison with a rule-based operation strategy

In order to compare the obtained results with a simpler, reference case, we implement a rule-based operation strategy (RBS) [13, 62]. The outline of the algorithm is shown in Fig.17. The principle is to use the HSS first, and if it is unavailable, to use the BSS. It should be noted that the algorithm does not try to maintain the SOC or LOH level for future use, contrary to the proposed algorithm. Case 1A is run again with the RBS. Results, also given in Table 3, show that because using HSS is cheaper, the operation cost is low, but then more BSS capacity is required to ensure power balance. As a consequence, the total capital cost is the largest of all cases.

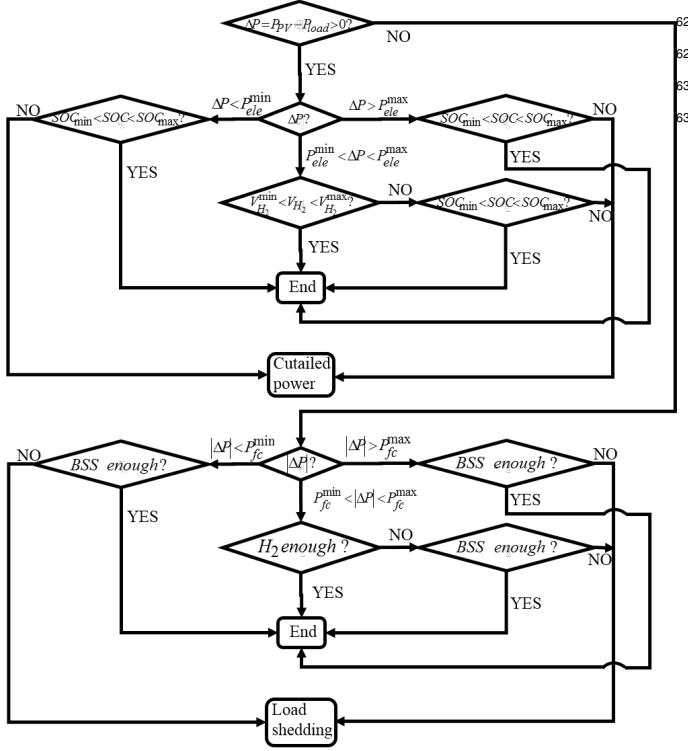


Figure 17: Rule-based strategy algorithm.

5.8. Influence of time resolution

In the above simulation, one-week average data is used. A better time resolution (for example, one day or one hour) may provide more accurate results; however, this would also significantly increase computation time to several days or more. In order to check the validity of the obtained results with more precise input data, a rolling-horizon scheduling simulation with a 1-hour time resolution is conducted. This resolution is selected as it is the maximum resolution available for the input data. In summary, the algorithm runs a scheduling task with 1-hour data over 1 day, and repeats this every day for a year.

Results are shown in Figs. 18 (SOC, LOH, LS and PVC) and 19 (scheduling results from 2000 hour to 2300 hour). From these curves, it can be observed that large LS and PVC occur during some periods of the year. As LS and PVC use are supposed to remain rare, this means that the sizing results are insufficient. A reason for this result is that the average data reflects the average load in the system, but does not consider peak load situations. A similar reasoning may be used for PV generation.

In order to adjust sizing results, the difference between PV output and load demand is computed and shown in Fig. 20. Then we adopt the maximum shortage value (i.e., the minimum value in Fig. 20) as the capacity of fuel cell, and the maximum surplus value (i.e., the maximum value in Fig. 20) as the capacity of electrolyzer. And sizing value of the HSS are adjusted, so that $P_{fc}^{max} = 13$, $P_{ele}^{max} = 37$.

After this adjustment, the rolling-horizon simulation is run again. Fig. 21 shows the resulting SOC, LOH, LS and PVC, and Fig. 22 shows the scheduling results from 2000 hour to 2300 hour with the new sizing values. After adjusting the sizing

value based on the peak load demand, no LS or PVC occur. And with the adjusted sizing values, we run MILP scheduling for case1A, and total cost is €212160, operation cost C_{op} is €1788.7, and capital cost C_{cap} is €138080.

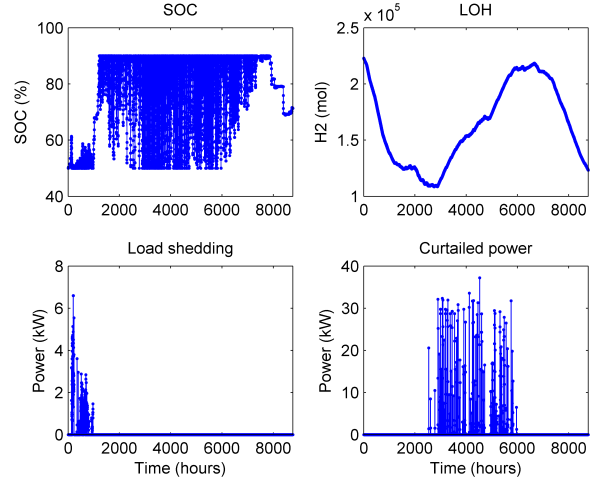


Figure 18: One-hour one-day rolling horizon scheduling simulation.

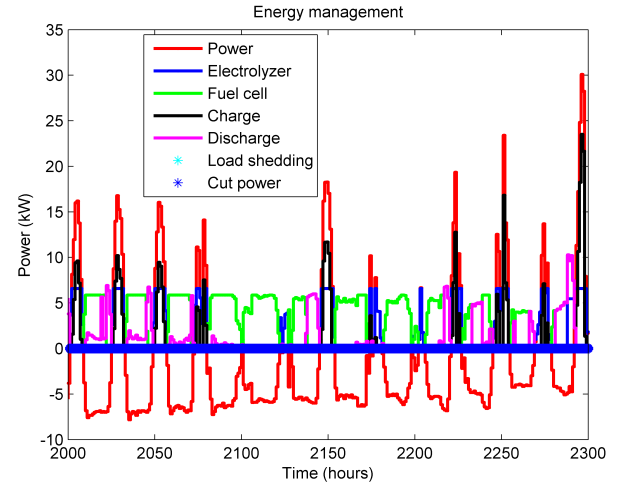


Figure 19: One-hour one-day rolling horizon scheduling simulation (2000 h-2300 h). The curve labelled 'Power' corresponds to the PV output minus the load.

5.9. Influence of uncertainty

As discussed earlier, uncertainty on forecasts of PV output and load can impact sizing results. To account for this uncertainty, the upper bound and lower bounds of estimated values are used. In the following, $\widetilde{P}_{PV}(t)$ and $\widetilde{P}_{load}(t)$ are the actual PV output and load values, and Er_{PV} and Er_{load} the error on PV output and load, respectively. The lower and upper bounds are then obtained with $\widetilde{P}_{PV}(t) = P_{PV}(t) \pm P_{PV}(t) \cdot Er_{PV}$ and $\widetilde{P}_{load}(t) = P_{load}(t) \pm P_{load}(t) \cdot Er_{load}$.

Two cases are defined. The worst case (the case where the difference between PV output and load is the largest) is when

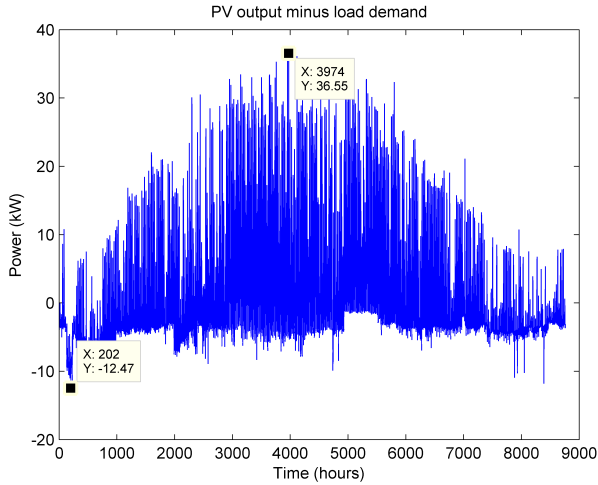


Figure 20: PV output minus load demand.

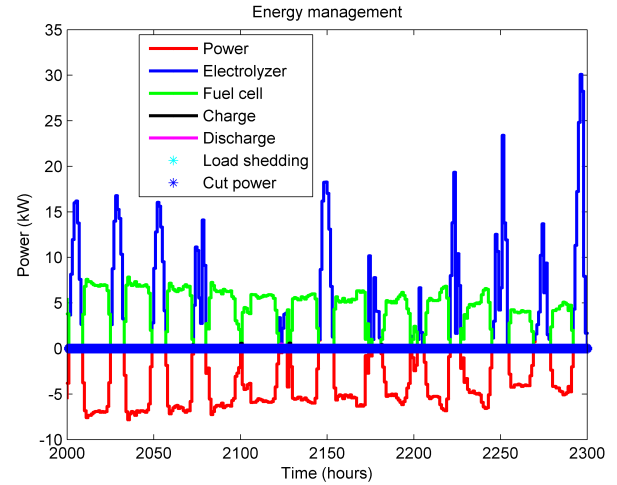


Figure 22: One-hour one-day rolling horizon scheduling simulation with the new sizing value of HSS (2000 h-2300 h). The curve labelled 'Power' corresponds to the PV output minus the load.

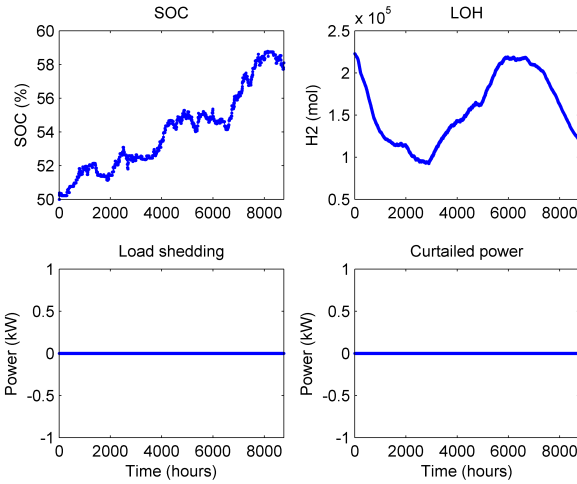


Figure 21: One-hour one-day rolling horizon scheduling simulation with the new sizing value of HSS.

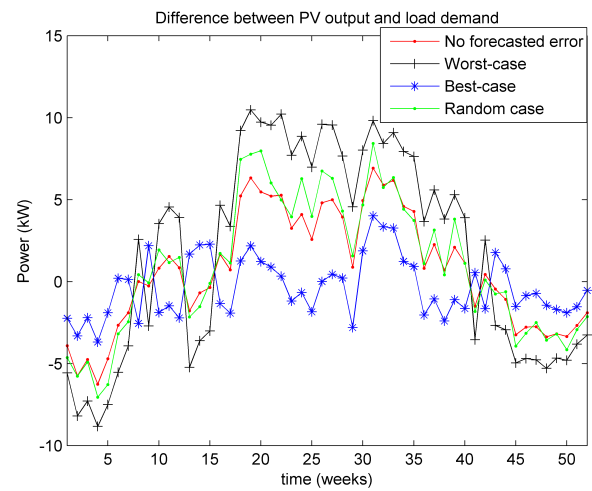


Figure 23: Difference between PV output and load demand in 4 cases.

PV output is equal to the upper bound value, and load is equal to the lower bound value; or when PV output is equal to the lower bound value, load is equal to the upper bound value. For the best case (the case where the difference between PV output and load is the lowest), the opposite is used.

Values for $\widetilde{P}_{PV}(t)$ minus $\widetilde{P}_{load}(t)$ are shown in Fig. 23. If the sizing results can satisfy the worst and best cases, then others cases can also be satisfying by the obtained sizing results. This means that the worst and best case data must be used to run the co-optimization method and obtain the sizing results. Table 5 shows the sizing results when $Er_{PV} = Er_{load} = 0.1$. For the worst-case, the HSS used frequently because it is cheaper than BSS. For the best case, the BSS is used frequently due to limitations of the HSS (minimum startup power), so more BSS capacity is needed.

6. Conclusion

In this paper, we present a methodology to determine the optimal sizing for a stand-alone microgrid. This methodology combines an EA for sizing and MILP for scheduling, and enables considering advanced energy management strategies, capable of anticipating decisions (especially with respect to storage), compared to classical rule-based approaches. Results show that the operation strategy, initial conditions, time resolution as well as uncertainty on input data influence the sizing of the components, and consequently the total cost of the microgrid. A comparison with a rule-based operation strategy is run, and sizing results show that co-optimization method performs better. A rolling-horizon simulation is used to adjust the sizing values due to the influence of input data time resolution. At last, forecasting errors are taken into account using a robust method, to further adjust sizing results. With the proposed method and complements, the proposed method can therefore be used for

Table 5: Sizing results considering uncertainty. The worst case is defined as the case where the difference between PV output and load is the largest, and the lowest for the best case.

Case	Total Cost [€]	C_{op} [€]	C_{cap} [€]	N_{PV}	P_{fc}^{max} [kW]	P_{el}^{max} [kW]	V_{H_2} [N.m ³]	C_{bat} [kWh]
Worst case	279270	1761.7	166960	50	8	8	11022	11
Best case	174400	1617.2	113450	50	6	6	5875	269

economically sizing a microgrid containing PV panels, a BSS and an HSS.

7. References

- [1] N. Lidula, A. Rajapakse, Microgrids research: A review of experimental microgrids and test systems, *Renewable and Sustainable Energy Reviews* 15 (1) (2011) 186–202.
- [2] N. Hatzigargyriou, H. Asano, R. Iravani, C. Marnay, *Microgrids, power and energy magazine* 5 (4) (2007) 78–94.
- [3] Y. A. Katsigiannis, P. S. Georgilakis, E. S. Karapidakis, Hybrid simulated annealing-tabu search method for optimal sizing of autonomous power systems with renewables, *Sustainable Energy, IEEE Transactions on* 3 (3) (2012) 330–338.
- [4] G. Kyriakarakos, A. I. Dounis, S. Rozakis, K. G. Arvanitis, G. Papadakis, Polygeneration microgrids: a viable solution in remote areas for supplying power, potable water and hydrogen as transportation fuel, *Applied Energy* 88 (12) (2011) 4517–4526.
- [5] Y. Wang, C. Chen, J. Wang, R. Baldick, Research on resilience of power systems under natural disasters—a review, *IEEE Transactions on Power Systems* 31 (2) (2016) 1604–1613.
- [6] C. Abbey, D. Cornforth, N. Hatzigargyriou, K. Hirose, A. Kwasinski, E. Kyriakides, G. Platt, L. Reyes, S. Suryanarayanan, Powering through the storm: microgrids operation for more efficient disaster recovery, *IEEE power and energy magazine* 12 (3) (2014) 67–76.
- [7] A. A. Akhil, G. Huff, A. B. Currier, B. C. Kaun, D. M. Rastler, S. B. Chen, A. L. Cotter, D. T. Bradshaw, W. D. Gauntlett, *Electricity storage handbook*, Tech. rep., DOE/EPRI in collaboration with NRECA (2013).
- [8] G. Kyriakarakos, D. D. Piromalis, K. G. Arvanitis, A. I. Dounis, G. Papadakis, On battery-less autonomous polygeneration microgrids: Investigation of the combined hybrid capacitors/hydrogen alternative, *Energy Conversion and Management* 91 (2015) 405–415.
- [9] G. Cau, D. Cocco, M. Petrollese, S. K. Kær, C. Milan, Energy management strategy based on short-term generation scheduling for a renewable microgrid using a hydrogen storage system, *Energy Conversion and Management* 87 (2014) 820–831.
- [10] J. Larminie, A. Dicks, M. S. McDonald, *Fuel cell systems explained*, Vol. 2, Wiley New York, 2003.
- [11] S. G. Tesfahunegn, Fuel cell assisted photovoltaic power systems.
- [12] T. Lajnef, S. Abid, A. Ammous, Modeling, control, and simulation of a solar hydrogen/fuel cell hybrid energy system for grid-connected applications, *Advances in Power Electronics* 2013.
- [13] M. Uzunoglu, O. Onar, M. Alam, Modeling, control and simulation of a pv/fc/uc based hybrid power generation system for stand-alone applications, *Renewable Energy* 34 (3) (2009) 509–520.
- [14] R. P. Menon, M. Paolone, F. Maréchal, Study of optimal design of polygeneration systems in optimal control strategies, *Energy* 55 (2013) 134–141.
- [15] A. Maleki, F. Pourfayaz, Optimal sizing of autonomous hybrid photovoltaic/wind/battery power system with lpsp technology by using evolutionary algorithms, *Solar Energy* 115 (2015) 471–483.
- [16] W. Zhou, C. Lou, Z. Li, L. Lu, H. Yang, Current status of research on optimum sizing of stand-alone hybrid solar–wind power generation systems, *Applied Energy* 87 (2) (2010) 380–389.
- [17] D. Connolly, H. Lund, B. V. Mathiesen, M. Leahy, A review of computer tools for analysing the integration of renewable energy into various energy systems, *Applied Energy* 87 (4) (2010) 1059–1082.
- [18] A. Maleki, A. Askarzadeh, Comparative study of artificial intelligence techniques for sizing of a hydrogen-based stand-alone photovoltaic/wind hybrid system, *international journal of hydrogen energy* 39 (19) (2014) 9973–9984.
- [19] A. Fetanat, E. Khorasaninejad, Size optimization for hybrid photovoltaic–wind energy system using ant colony optimization for continuous domains based integer programming, *Applied Soft Computing* 31 (2015) 196–209.
- [20] A. Maleki, A. Askarzadeh, Artificial bee swarm optimization for optimum sizing of a stand-alone pv/wt/fc hybrid system considering lpsp concept, *Solar Energy* 107 (2014) 227–235.
- [21] A. Maleki, M. Ameri, F. Keynia, Scrutiny of multifarious particle swarm optimization for finding the optimal size of a pv/wind/battery hybrid system, *Renewable Energy* 80 (2015) 552–563.
- [22] B. Zhao, X. Zhang, P. Li, K. Wang, M. Xue, C. Wang, Optimal sizing, operating strategy and operational experience of a stand-alone microgrid on dongfushan island, *Applied Energy* 113 (2014) 1656–1666.
- [23] R. Atia, N. Yamada, Optimization of a pv-wind-diesel system using a hybrid genetic algorithm, in: *Electrical Power and Energy Conference (EPEC)*, 2012 IEEE, IEEE, 2012, pp. 80–85.
- [24] B. Bahmani-Firouzi, R. Azizpanah-Abarghoee, Optimal sizing of battery energy storage for micro-grid operation management using a new improved bat algorithm, *International Journal of Electrical Power & Energy Systems* 56 (2014) 42–54.
- [25] C.-S. Karavas, G. Kyriakarakos, K. G. Arvanitis, G. Papadakis, A multi-agent decentralized energy management system based on distributed intelligence for the design and control of autonomous polygeneration microgrids, *Energy Conversion and Management* 103 (2015) 166–179.
- [26] M. Marzband, M. Javadi, J. L. Dominguez-Garcia, M. M. Moghaddam, Non-cooperative game theory based energy management systems for energy district in the retail market considering der uncertainties, *IET Generation, Transmission & Distribution*.
- [27] M. Marzband, N. Parhizi, M. Savaghebi, J. M. Guerrero, Distributed smart decision-making for a multimicrogrid system based on a hierarchical interactive architecture, *IEEE Transactions on Energy Conversion* 31 (2) (2016) 637–648.
- [28] M. Marzband, F. Azarinejadian, M. Savaghebi, J. M. Guerrero, An optimal energy management system for islanded microgrids based on multi-period artificial bee colony combined with markov chain, *IEEE SYSTEMS JOURNAL*.
- [29] M. Marzband, E. Yousefnejad, A. Sumper, J. L. Domínguez-García, Real time experimental implementation of optimum energy management system in standalone microgrid by using multi-layer ant colony optimization, *International Journal of Electrical Power & Energy Systems* 75 (2016) 265–274.
- [30] M. Marzband, M. Ghadimi, A. Sumper, J. L. Domínguez-García, Experimental validation of a real-time energy management system using multi-period gravitational search algorithm for microgrids in islanded mode, *Applied energy* 128 (2014) 164–174.
- [31] M. Marzband, N. Parhizi, J. Adabi, Optimal energy management for stand-alone microgrids based on multi-period imperialist competition algorithm considering uncertainties: experimental validation, *International transactions on electrical energy systems*.
- [32] M. Marzband, A. Sumper, A. Ruiz-Álvarez, J. L. Domínguez-García, B. Tomoiagă, Experimental evaluation of a real time energy management system for stand-alone microgrids in day-ahead markets, *Applied Energy* 106 (2013) 365–376.
- [33] P. Murty, *Operation and control in power systems*, BS Publications, 2011.
- [34] R. Hemmati, H. Saboori, Short-term bulk energy storage system scheduling for load leveling in unit commitment: modeling, optimization, and sensitivity analysis, *Journal of advanced research* 7 (3) (2016) 360–372.
- [35] K. P. Detroja, Optimal autonomous microgrid operation: A holistic view, *Applied Energy* 173 (2016) 320–330.
- [36] L. Guo, W. Liu, J. Cai, B. Hong, C. Wang, A two-stage optimal planning and design method for combined cooling, heat and power microgrid

- system, *Energy Conversion and Management* 74 (2013) 433–445. ⁸⁶⁶
- [37] J. S. Kim, T. F. Edgar, Optimal scheduling of combined heat and power plants using mixed-integer nonlinear programming, *Energy* 77 (2014) 675–690. ⁸⁶⁷
⁸⁶⁸
⁸⁶⁹
- [38] M. Marzband, A. Sumper, J. L. Domínguez-García, R. Gumara-Ferret, Experimental validation of a real time energy management system for microgrids in islanded mode using a local day-ahead electricity market and minlp, *Energy Conversion and Management* 76 (2013) 314–322. ⁸⁷⁰
⁸⁷¹
⁸⁷²
- [39] H. Daneshi, A. K. Srivastava, Security-constrained unit commitment with wind generation and compressed air energy storage, *Generation, Transmission & Distribution, IET* 6 (2) (2012) 167–175. ⁸⁷³
⁸⁷⁴
⁸⁷⁵
⁸⁷⁶
- [40] R. Palma-Behnke, C. Benavides, F. Lanas, B. Severino, L. Reyes, J. Llanos, D. Sáez, A microgrid energy management system based on the rolling horizon strategy, *Smart Grid, IEEE Transactions on* 4 (2) (2013) 996–1006. ⁸⁷⁷
⁸⁷⁸
⁸⁷⁹
- [41] S. Parhoudeh, A. Baziar, A. Mazareie, A. Kavousi-Fard, A novel stochastic framework based on fuzzy cloud theory for modeling uncertainty in the micro-grids, *International Journal of Electrical Power & Energy Systems* 80 (2016) 73–80. ⁸⁸⁰
⁸⁸¹
⁸⁸²
- [42] A. Zakariazadeh, S. Jadid, P. Siano, Smart microgrid energy and reserve scheduling with demand response using stochastic optimization, *International Journal of Electrical Power & Energy Systems* 63 (2014) 523–533. ⁸⁸³
⁸⁸⁴
- [43] Y. Xiang, J. Liu, Y. Liu, Robust energy management of microgrid with uncertain renewable generation and load, *IEEE Transactions on Smart Grid* 7 (2) (2016) 1034–1043. ⁸⁸⁵
⁸⁸⁶
⁸⁸⁷
- [44] E. Kuznetsova, Y.-F. Li, C. Ruiz, E. Zio, An integrated framework of agent-based modelling and robust optimization for microgrid energy management, *Applied Energy* 129 (2014) 70–88. ⁸⁸⁸
⁸⁸⁹
⁸⁹⁰
- [45] A. Hussain, V.-H. Bui, H.-M. Kim, Robust optimization-based scheduling of multi-microgrids considering uncertainties, *Energies* 9 (4) (2016) 278. ⁸⁹¹
⁸⁹²
- [46] G. Liu, K. Tomsovic, Robust unit commitment considering uncertain demand response, *Electric Power Systems Research* 119 (2015) 126–137. ⁸⁹³
⁸⁹⁴
- [47] F. Valencia, J. Collado, D. Sáez, L. G. Marín, Robust energy management system for a microgrid based on a fuzzy prediction interval model, *IEEE Transactions on Smart Grid* 7 (3) (2016) 1486–1494. ⁸⁹⁵
⁸⁹⁶
⁸⁹⁷
- [48] R. Dufo-Lopez, J. L. Bernal-Agustín, J. Contreras, Optimization of control strategies for stand-alone renewable energy systems with hydrogen storage, *Renewable energy* 32 (7) (2007) 1102–1126. ⁸⁹⁸
⁸⁹⁹
⁹⁰⁰
- [49] A. Khodaei, M. Shahidehpour, Microgrid-based co-optimization of generation and transmission planning in power systems, *IEEE transactions on power systems* 28 (2) (2013) 1582–1590. ⁹⁰¹
⁹⁰²
- [50] A. Khodaei, S. Bahramirad, M. Shahidehpour, Microgrid planning under uncertainty, *IEEE Transactions on Power Systems* 30 (5) (2015) 2417–2425. ⁹⁰³
⁹⁰⁴
⁹⁰⁵
- [51] J. Zhang, K.-J. Li, M. Wang, W.-J. Lee, H. Gao, A bi-level program for the planning of an islanded microgrid including caes, in: *Industry Applications Society Annual Meeting, 2015 IEEE*, IEEE, 2015, pp. 1–8. ⁹⁰⁶
⁹⁰⁷
⁹⁰⁸
- [52] L. Xu, X. Ruan, C. Mao, B. Zhang, Y. Luo, An improved optimal sizing method for wind-solar-battery hybrid power system, *Sustainable Energy, IEEE Transactions on* 4 (3) (2013) 774–785. ⁹⁰⁹
⁹¹⁰
⁹¹¹
- [53] P. Diéguez, A. Urstúa, P. Sanchis, C. Sopena, E. Guelbenzu, L. Gandía, Thermal performance of a commercial alkaline water electrolyzer: experimental study and mathematical modeling, *international journal of hydrogen energy* 33 (24) (2008) 7338–7354. ⁹¹²
⁹¹³
⁹¹⁴
- [54] Ø. Ulleberg, Modeling of advanced alkaline electrolyzers: a system simulation approach, *International journal of hydrogen energy* 28 (1) (2003) 21–33. ⁹¹⁵
⁹¹⁶
⁹¹⁷
- [55] F. Laurencelle, R. Chahine, J. Hamelin, K. Agbossou, M. Fournier, T. Bose, A. Laperriere, Characterization of a ballard mk5-e proton exchange membrane fuel cell stack, *Fuel Cells* 1 (1) (2001) 66–71. ⁹¹⁸
⁹¹⁹
⁹²⁰
- [56] F. Garcia, C. Bordons, Optimal economic dispatch for renewable energy microgrids with hybrid storage using model predictive control, in: *Industrial Electronics Society, IECON 2013-39th Annual Conference of the IEEE*, IEEE, 2013, pp. 7932–7937. ⁹²¹
⁹²²
⁹²³
- [57] T. M. Hansen, R. Roche, S. Suryanarayanan, A. A. Maciejewski, H. J. Siegel, Heuristic optimization for an aggregator-based resource allocation in the smart grid, *IEEE Transactions on Smart Grid* 6 (4) (2015) 1785–1794. doi:10.1109/TSG.2015.2399359. ⁹²⁴
⁹²⁵
⁹²⁶
- [58] R. Roche, S. Suryanarayanan, T. M. Hansen, S. Kiliccote, A. Miraoui, A multi-agent model and strategy for residential demand response coordination, in: *PowerTech, 2015 IEEE Eindhoven*, 2015, pp. 1–6. doi:10.1109/PTC.2015.7232268. ⁹²⁷
⁹²⁸
⁹²⁹
- [59] G. Ferrari-Trecate, E. Gallestey, P. Letizia, M. Spedicato, M. Morari, M. Antoine, Modeling and control of co-generation power plants: a hybrid system approach, *IEEE Transactions on Control Systems Technology* 12 (5) (2004) 694–705. ⁹³⁰
⁹³¹
⁹³²
- [60] B. Colson, P. Marcotte, G. Savard, An overview of bilevel optimization, *Annals of operations research* 153 (1) (2007) 235–256. ⁹³³
⁹³⁴
- [61] J. Lagorse, D. Paire, A. Miraoui, Sizing optimization of a stand-alone street lighting system powered by a hybrid system using fuel cell, {PV} and battery, *Renewable Energy* 34 (3) (2009) 683–691. ⁹³⁵
⁹³⁶
⁹³⁷
- [62] M. Castañeda, A. Cano, F. Jurado, H. Sanchez, L. M. Fernandez, Sizing optimization, dynamic modeling and energy management strategies of a stand-alone pv/hydrogen/battery-based hybrid system, *International journal of hydrogen energy* 38 (10) (2013) 3830–3845. ⁹³⁸
⁹³⁹
⁹⁴⁰